Matsumura et al. BMC Zoology (2020) 5:9
https://doi.org/10.1186/s40850-020-00058-2

BMC Zoology

RESEARCH ARTICLE Open Access

3D printed spermathecae as experimental models to understand sperm dynamics in leaf beetles

Yoko Matsumura*, Sinje Gürke, Halvor T. Tramsen and Stanislav N. Gorb

Abstract

Background: Postcopulatory mate choice occurs ubiquitously in the animal kingdom. However, it is usually a major challenge to visualise the process taking place in a body. This fact makes it difficult to understand the mechanisms of the process. By focusing on the shape of female sperm storage organs (spermathecae), we aimed to elucidate their functional morphology using six representative beetle species and to simulate sperm dynamics in artificial spermathecae with different structural features.

Results: Morphology and material gradients were studied using micro-computed tomography (μCT) and confocal laser scanning microscopy. This study shows a diversity of external and internal structures of the spermathecae among species. Despite the diversity, all species possess a common pumping region, which is composed of a sclerotised chamber, muscles and a resilin-enriched region. By focusing on the species *Agelastica alni*, whose spermatheca is relatively simple in shape with an internal protuberance, we simulated sperm dynamics by establishing a fabrication method to create enlarged, transparent, flexible and low-cost 3D models of biological structures based on μCT data. This experiment shows that the internal protuberance in the species functions as an efficient mixing device of stored sperm.

Conclusions: The observed spermathecal musculature implies that the sclerotised chamber of the spermatheca with muscles works as a pumping organ. Our fluid dynamics tests based on 3D printed spermathecae show that a tiny structural difference causes entirely different fluid dynamics in the spermatheca models. This result suggests that structural variations of the spermatheca strongly affect sperm dynamics. However, fluid dynamics tests still require essential measurements including sperm viscosity and the velocity of pumping cycles of the spermatheca.

Keywords: Beetles, Fluid dynamics, Insects, Sexual selection, Sperm storage organs

Background

Animals are frequently polyandrous [1], and females can often store sperm received during mating with different males [2, 3]. Thus, mating success does not guarantee male reproductive success, and postcopulatory sexual selection (PCSS) takes place [3–8]. The main sexual selection mechanisms are sperm competition [7, 8], sexual conflict [9] and cryptic female choice (CFC) [5, 10, 11]. PCSS by these mechanisms is not mutually exclusive [12–15], but the theoretical importance of clear definitions was discussed in Brennan and Prum [16]. For instance, it is not always easy to distinguish whether male paternity biases are caused either by differentially allocated sperm placed by males or through female control of sperm allocation [12, 13, 15]. Moreover, sexual selection through one mechanism can be an evolutionary driving force of the other mechanisms, e.g., cryptic female choice could promote

* Correspondence: yoko.matumura.hamupeni@gmail.com; ymatsumura@zoologie.uni-kiel.de
Department of Functional Morphology and Biomechanics, Zoological Institute, Kiel University, Am Botanischen Garten 1–9, 24118 Kiel, Germany

developing a male preference/character that is harmful to females [12, 14]. To further disentangle these highly complicated mechanisms causing PCSS, we must (1) increase the number of case studies verifying the selection mechanisms [13, 15] and (2) unveil evolutionary histories of PCSS [12].

CFC occurs within a female body, where it is usually challenging to observe, and this makes it difficult to understand the mechanisms of this process [12]. A well-known and visible example of CFC is sperm ejection by females during and after copulation, e.g., as observed in waterfowls [17], kittiwakes [18], insects [19] and spiders [20]. In addition, numerous other processes contributing to CFC have been hypothesised, discussed and at least partly but experimentally demonstrated [6, 10, 13, 21]. Firman et al. [6] summarised different mechanisms of CFC occurring in reproductive processes: time of insemination, ejaculation size, sperm ejection, sperm neutralisation, sperm storage, sperm dumping, sperm activation, attraction to eggs and finally fertilisation. This diversity implies that female reproductive organs always play important roles. However, researchers traditionally tended to study females less than males [14, 22, 23].

A sperm storage organ is a part of the female reproductive organs, where CFC takes place. Female sperm storage organs, termed either *spermathecae* or *receptaculum seminis*, are present in a wide range of animal taxa including arthropods, molluscs, annelids, nematodes and amphibians [2, 24]. The number of these organs varies among taxa. For example, fruit flies and dung flies possess multiple spermathecae, and females alter paternity patterns by using them e.g., [25, 26]. However, the majority of insects have just one spermatheca [24]. In some beetles, it was experimentally confirmed that the spermatheca enables females to control sperm allocation and usage e.g., [27–29]. The spermatheca in some insects is well sclerotised, and its structural variation has been used in systematics and phylogenetic studies [30–34]. Based on a comparative approach, Higginson et al. [35] ascertained that female reproductive tract architecture likely drives diversification of sperm morphology in diving beetles. These facts led us to the following questions: (1) how does the morphological diversity found in the spermathecae affect CFC and (2) what roles does it play in the evolution of CFC? Considering the invisibility and complexity of the postcopulatory processes in many animals, we have to apply an integrative approach based on different aspects and experimental techniques [36, 37].

Functional morphology and biomechanics approaches are often missing in sexual selection studies and have just started to be applied in recent research [38, 39]. Here, we try to verify the functional significance of the structural diversity of the spermatheca in the beetle family Chrysomelidae. In systematics of Chrysomelidae, the spermatheca is often described, and its significance for species identification is accepted e.g., [30, 33, 40, 41]. We selected common species that we can collect easily in large numbers and whose mating behaviour we can often observe in the field, although their mating rates are not yet known. To achieve our purpose, we applied micro-computed tomography (μCT) for the spermatheca to describe its 3D morphology including the detailed internal structures. We investigated the musculature and material distribution within the spermatheca to discuss the functional morphology of this organ. Additionally, we simulated the sperm dynamics in the spermatheca experimentally by utilising printed 3D models. Based on these experimental results, we discuss how the spermatheca works and contributes to CFC. Even though a physical characterisation of semen is missing (e.g., viscosity and its importance were already pointed out in Werner and Simmons [42]), our approach attempts to show that the structural variations of the spermatheca may influence sperm dynamics.

Results

Morphology

We investigated the morphology of the spermatheca from six representative species using μCT and a scanning electron microscope (SEM). The following six chrysomelid species from four subfamilies were used for these experiments: *Cassida vibex* Linnaeus, 1767 (Cassidinae), *Agelastica alni* (Linnaeus, 1758) (Galerucinae), *Gastrophysa viridula* (DeGeer, 1775) (Galerucinae), *Donacia crassipes* Fabricius, 1775 (Donaciinae), *Crioceris duodecimpunctata* (Linnaeus, 1758) (Criocerinae) and *Crioceris asparagi* (Linnaeus, 1758) (Criocerinae). The terminology used below is not based on a homology assessment (Fig. 1a, b). However, we considered the terminology to be helpful for readers to understand the morphology because the opening of the spermathecal gland is an unmistakable landmark to demarcate its distal and proximal parts (Fig. 1a, b, white arrowheads).

The spermathecae in the studied species are sclerotised and melanised. The spermatheca comprises a C-shaped distal part carrying a gland at its proximal end and an interspecific highly variable proximal part connected to the spermathecal duct at its proximal end (Fig. 1). Muscle fibres are connected either to two C-arms (Fig. 2a-d) or to a distal C-arm and the beginning of the proximal part (Fig. 2e, f). The shape of the spermatheca is species specific, although intraspecific variations were also found in spirals of Ca. *vibex* and loops of *Cr. asparagi*, *Cr. duodecimpunctata* and *G. viridula* (see Figs. 1, 2 and 3). The species-specific features are summarised in Table 1. Characters representing those species-specific features are the (1)

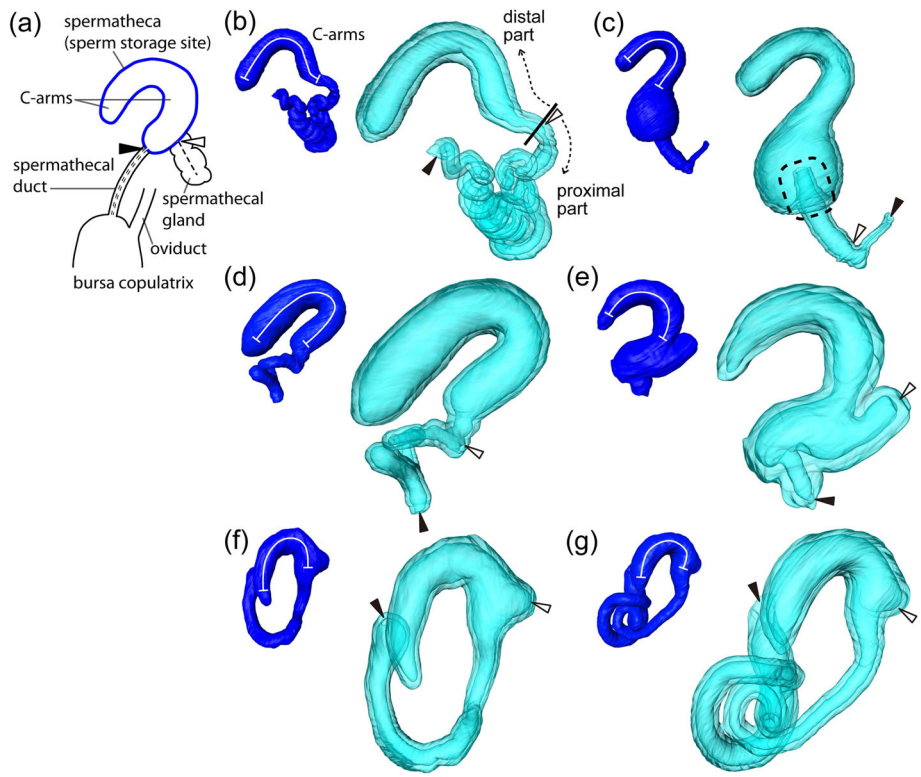

Fig. 1 3D external (blue) and internal (light blue and semi-transparent) morphology of spermathecae. **a** Scheme of a part of the female reproductive system. **b** *Cassida vibex*. **c** *Agelastica alni*. **d** *Gastrophysa viridula*. **e** *Donacia crassipes*. **f** *Crioceris duodecimpunctata*. **g** *Cr. asparagi*. The position of the gland opening was used to demarcate proximal and distal parts of the spermathecae. The white arrowheads point to the openings of the spermathecal gland, and the black arrowheads denote the openings of the spermathecal duct

distances of two C-arms, (2) relative lengths of the two C-arms, (3) relative sizes of the lumen of the entire spermatheca, (4) presence/absence of remarkable internal structures, (5) shapes of the proximal part, (6) presence/absence of additional sperm storage spaces and (7) relative sizes of the entrance of the spermathecal duct in comparison to the lumen size.

Material gradients

To investigate material gradients in the spermatheca, we applied the method developed by Michels and Gorb [43] using confocal laser scanning microscopy (CLSM). We visualised the autofluorescence of materials and compared spermathecae using four sets of emitting wavelengths and emission filters. Then, we assigned the micrograph colours as blue, green, red (50% saturation) and red (50% saturation). Following Michels and Gorb [43], we interpreted each overlaid micrograph and described the physical properties of the spermatheca as follows: well sclerotised (red), relatively well sclerotised and flexible (yellow to green) and rubber-like protein resilin enriched (blue).

Material gradient analyses showed a similar tendency among the studied species apart from *A. alni* (Fig. 2). The spermatheca of *A. alni* is well melanised, a large part of the distal area did not exhibit much autofluorescence intensity, and the information remained unclear (Fig. 2b). The spermathecae of the other studied species have a blue-coloured region in the middle of the C-arms. This observation suggests that a large proportion of the rubber-like protein resilin is present there (Fig. 2a, c-f). This part was homogeneously resilin dominated in Ca. *vibex* and *D. crassipes* (Fig. 2a, d), while a material gradient from the outer curve to the inner curve was observed in *G. viridula*, *Cr. duodecimpunctata* and *Cr. asparagi* (Fig. 2c, e, f). Other areas were visualised with green to red, which suggests that those areas are well sclerotised.

Fluid dynamics tests

To experimentally simulate sperm dynamics, we created enlarged, transparent and flexible spermatheca models (see "Preparation of models" below) and performed fluid dynamics tests under a conventional 3D printer. To simulate sperm dynamics in the scaled-up models, we had to take the Reynolds number into account and needed to adjust the viscosity of a medium for the experiments (see "Fluid dynamics tests" below). However,

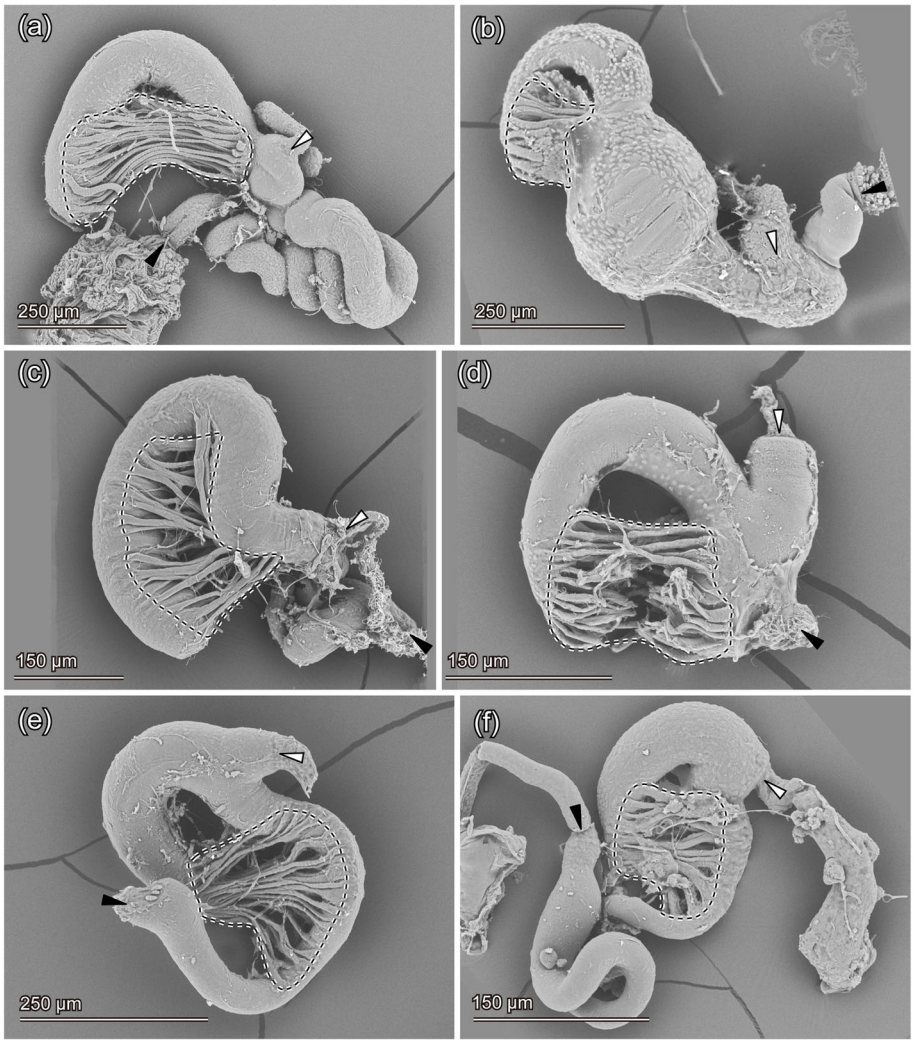

Fig. 2 Scanning electron micrographs of spermathecae. The white arrowheads point to the openings of the spermathecal gland, and the black arrowheads denote the openings of the spermathecal duct. Dashed lines encircle muscles. **a** *Cassida vibex*. **b** *Agelastica alni*. **c** *Gastrophysa viridula*. **d** *Donacia crassipes*. **e** *Crioceris duodecimpunctata*. **f** *Cr. asparagi*

the viscosity of sperm in insects is not known, and for simplicity, we assumed that it is equivalent to that of water. Then, we selected 1,2-propanediol (propylene glycol) as the medium for the following experiments.

For these experiments, we focused on one species and chose *A. alni* for the following two reasons. (1) Although the spermatheca of *A. alni* lacks information on material gradients due to a high pigmentation level, the fundamental morphology including muscle arrangements is similar to that of the other studied species discussed below, and the functional morphology of the spermatheca must be similar among the studied species. (2) Here, we aimed to visualise a qualitative difference in variable spermatheca models, and utilisation of the *A. alni* spermatheca-like model enables us to compare fluid dynamics between a realistic model with an internal protuberance and a modified model without the protuberance. We prepared two different types of spermatheca models with and without the internal protuberance to elucidate the functions of the internal protuberance observed in *A. alni*.

Our fluid dynamics tests demonstrate that the pumping C-arms cause inflows and outflows in both types of models with and without the internal protuberance (Fig. 4). These tests also show differences in the fluid dynamics between the models already at the first pumping cycle (Fig. 4 left vs. right columns, supplementary information 3, Movies 1 vs. 2). The outflow in the model with the protuberance remarkably occurs from the swollen part through the protuberance to the shaft region (relatively narrowed area of the proximal part) (Fig. 4c-f). In contrast, the outflow in the model without

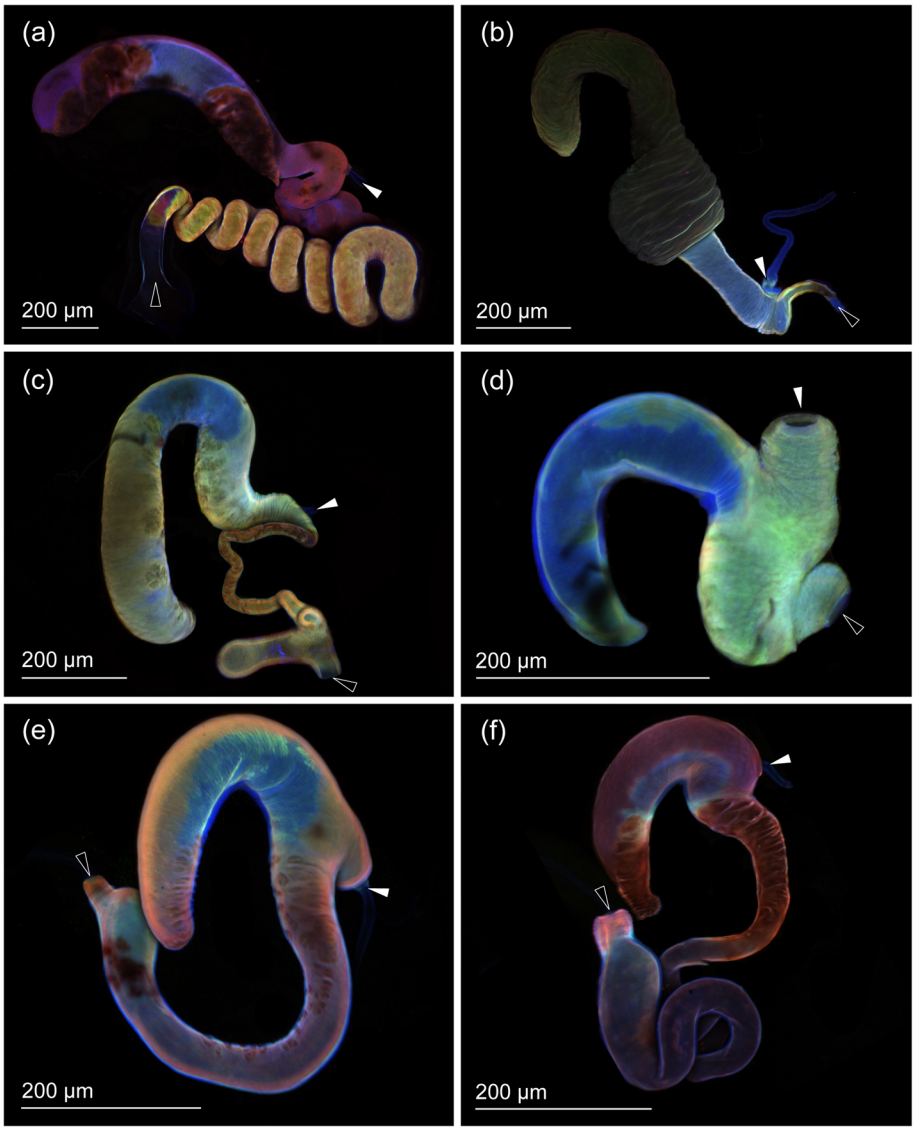

Fig. 3 Confocal laser scanning micrographs of spermathecae. The white arrowheads point to the openings of the spermathecal gland, and the black arrowheads denote the openings of the spermathecal duct. **a** *Cassida vibex*. **b** *Agelastica alni*. **c** *Gastrophysa viridula*. **d** *Donacia crassipes*. **e** *Crioceris duodecimpunctata*. **f** *Cr. asparagi*

the protuberance only takes place in the shaft region (Fig. 4c'-f'). The dynamic inflow within the first pumping cycle in the model with the protuberance happens again in the swollen part and shaft region (Fig. 4g-i). The inflow, moving from the shaft to the swollen part, apparently causes a vortex in the swollen part (Fig. 4g-i, k). This effect was more obviously observed in the inflow processes at the latter pumping cycles (Fig. 4j). In contrast, the inflow at the first pumping cycle in the model without the protuberance only takes place in the shaft (Fig. 4g'-i',k'). The inflow in the swollen part is slightly recognisable in the later cycles (Fig. 4j').

Subsequent still images taken after every 10 pumping cycles show that the injected ink spots are visible in a broader region in the model without the protuberance (Fig. 5a'-d') than in that with the protuberance (Fig. 5a-d) (compare the regions surrounded with the black solid lines in Fig. 5d, d').

The fluid dynamics mentioned above were observed in the experiments under a 3D printer, with which we controlled the velocity of pumping cycles. We also saw very similar results in the tests repeatedly performed by hand (Supplementary information 4, Fig. 1 left vs. right columns, Supplementary information 5, Movies 1 vs. 3, 2 vs. 4).

Discussion

Studies on female genitalia have been less carried out than those devoted to males because it was believed that

Table 1 External and internal morphology of the spermathecae in the studied species

	Cassida vibex	*Agelastica alni*	*Gastrophysa viridula*	*Donacia crassipes*	*Crioceris duodecimpunctata*	*Crioceris asparagi*
Distances of two C-arms	Wider in Ca. *vibex* than in other species					
Relative lengths of two C-arms	Equal	The proximal part is longer, and its middle part is swollen	The distal part is much longer	Equal, and the proximal part is slightly swollen	The distal part is longer, and the proximal part is slightly swollen	The distal part is longer, and the proximal part is slightly swollen
Relative sizes of the lumen	The lumen size of the distal part is more prominent in all species, and in *G. viridula* the difference is much bigger than the others					
Internal structures	Absent	Volcano-like protuberance at the middle	Absent	Absent	Absent	Absent
Shapes of the proximal part	Highly coiled	Relatively narrowed duct	Relatively very narrowed duct and convoluted	Very short duct	Relatively long and curved	Relatively long and convoluted/ partly coiled
Additional sperm storage spaces	Absent	Absent	Present at the end of the main spermatheca	Absent	Absent	Absent
Sizes of the entrance	Slightly tapering towards the entrance	Relatively narrowed duct	Slightly tapering towards the entrance	The diameter of the lumen at the entrance abruptly diminishes	The diameter of the lumen at the entrance abruptly diminishes	The diameter of the lumen at the entrance abruptly diminishes

the structural diversity of female reproductive organs is less remarkable than that of their male counterparts [22, 23, 38]. Nevertheless, co-evolution of male and female reproductive organs has been reported from a wide range of animal taxa [14, 38]. Phylogeny-based comparative studies in invertebrates have verified that in such co-evolution, not only male structures but also female structures play an active role [35, 44, 45].

Our study verified that the spermathecae in the studied species show high structural diversity not only in the external structures as previously described in systematics [30–34] but also in the internal structures. The studied species commonly have a sclerotised and C-shaped chamber carrying muscles situated between the C-arms or the distal C-arm and the beginning of the proximal part. At the middle of the C-shaped chamber, a resilin-enriched region was detected in all species except for *A. alni*, whose corresponding area is strongly melanised and barely emits autofluorescence. ölüölResilin is an elastomeric protein often found in arthropod cuticles. It provides cuticles with various functional advantages, e.g., (1) compliance enhancement, (2) elastic energy storage and (3) reduction of fatigue and damage [46]. Therefore, our functional interpretations of these specific morphological details of spermathecae are as follows. The muscles attaching to the C-arms contract and cause pumping cycles. The spermatheca needs to be relatively stiff so that its deformation cannot lose forces generated during the pumping cycles. These movements take place quite often, and stresses accumulate in structures situated between the C-arms. Therefore, this region is resilin-enriched to prevent any damage. These interpretations are partly underpinned by previous findings on the functions of similarly arranged spermathecal muscles verified in a weevil, i.e., sperm supply to eggs [29] and in a leaf beetle, i.e., sperm uptake after mating and sperm supply to eggs [28]. The C-shaped chamber with muscles is a pumping organ. On the other hand, it remains unclear why there are striking material gradients, not only resilin distributions, within a spermatheca and between species. For instance, two *Crioceris* species have a similar tendency (Fig. 2e, f), but the material gradient of *Donacia crassipes*, which belongs to Donaciinae, the sister subfamily of Criocerinae [47], does not look identical to that of the criocerine *Crioceris* species. This difference suggests that the observed material gradient does not necessarily reflect their phylogenetic relationship. Instead, it is conceivable that the material gradient reflects functional requirements.

The fluid dynamics tests using 3D printed spermatheca models of *A. alni* with and without the internal protuberance showed the potential value of our new approach. The two models used here have only a small structural difference. However, the observed fluid movements were remarkably different between the models, and the differences in fluid movements are summarised in Fig. 6. In the model without the protuberance, forces causing the outflows and inflows are attenuated due to

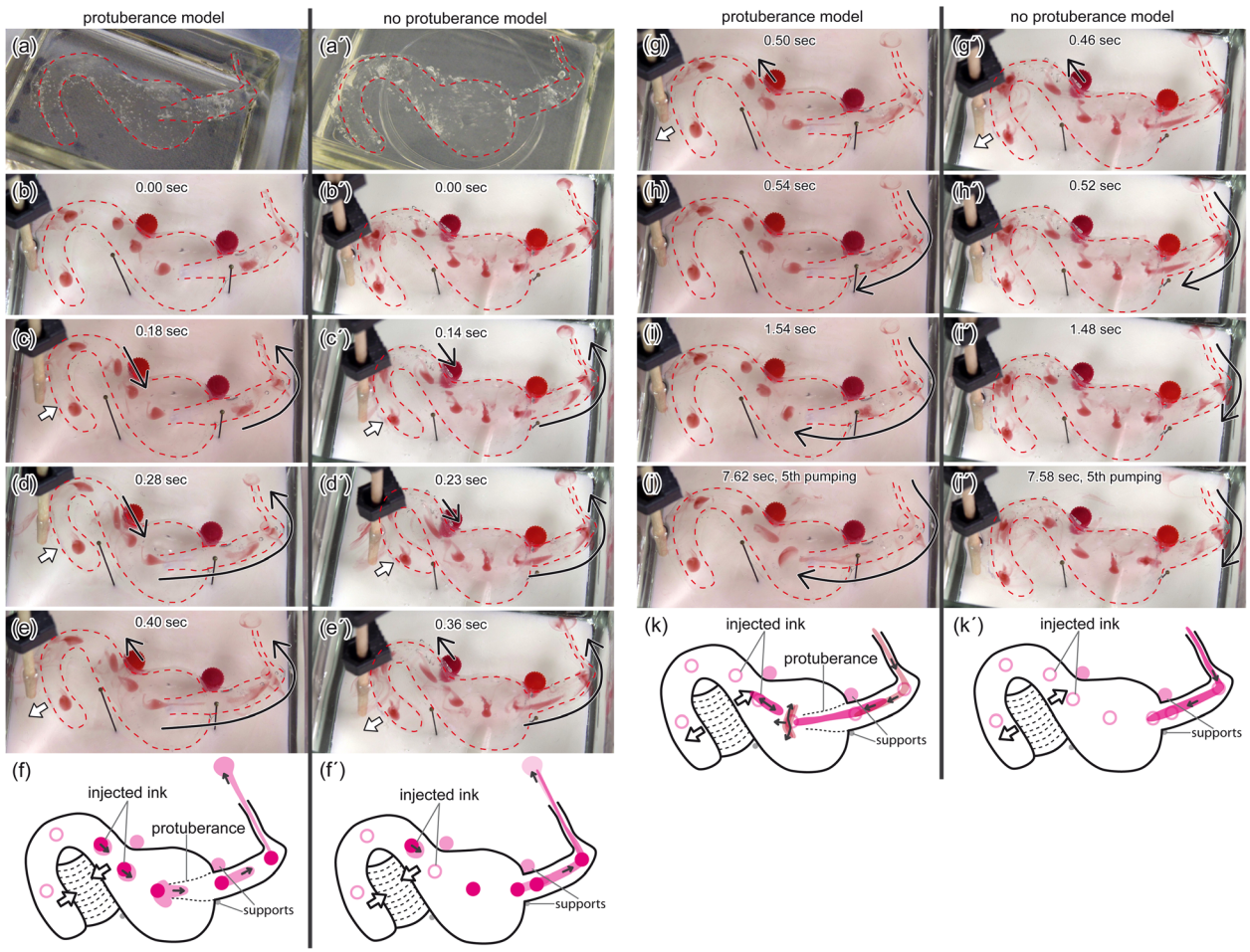

Fig. 4 Transparent flexible models and fluid dynamics tests (first pumping movement, outflow) using the *Agelastica alni* spermatheca models. With a realistic internal protuberance (left column) and without the protuberance (right column). **a-a'** The models fully immersed in 1,2-propanediol. **b-b'** Sudan Red in 1,2-propanediol was injected. **c-e'** The first pumping cycle performed was filmed at 50 fps, and still images showing different stages are exhibited. The solid white arrows indicate directions of the C-arm movement. The black arrows show a marked shift of the injected ink spots in the models. **f-f'** Schemes of the observed outflow in the first pumping cycle. Transparent flexible models and fluid dynamics tests (inflow) using the *Agelastica alni* spermatheca models. With a realistic internal protuberance (left column, highlighted with red dashed lines) and without the protuberance (right column). **g-i'** The first pumping filmed at 50 fps (**g-g'**: while pulling back the C-arm, **h-h'**: just after finishing pulling back the C-arm, **i-i'**: just before the second pumping cycle started), and still images showing different stages are presented. The solid white arrows show the direction of the distal C-arm movement. The black arrows show a marked shift of the fluid in the models. **j-j'** The inflow at the end of the 5th pumping cycle. **k-k'** Schemes of the observed inflow during the first five pumping cycles. The light-pink circles in the schemes indicate the original locations of the injected ink

the presence of the swollen part, and the resulting fluid movements in the model are relatively small. In contrast, due to the presence of the protuberance in the other model, the fluid dramatically moves at the interface between the protuberance and the swollen part. Although the pumping speed was not controlled entirely in our preliminary experiments (Supplementary information 4 and 5), we still repeatedly observed such differences between the models. Therefore, the function of the protuberance should be to mix fluids.

All studied species possess the C-shaped pumping chamber at the most distal part of the spermatheca, and in-between the chamber and spermathecal duct, the shape varies between species. The results of our fluid dynamics tests suggest that spermathecal shapes may play a role in changing the allocation of sperm in the spermatheca. Polyandry is more or less universal in animals [1], and sperm from different partners is stored in female sperm storage organs [2, 3]. Considering the very high fecundity in the species *A. alni* [48], it can be crucial that females acquire higher genetic diversity of their offspring. Therefore, at least some of the offspring can survive under unexpected conditions. The degree of polyandry is variable among species or even among individuals [1, 4], and interval lengths between successive mating also affect male fertilisation success. In general,

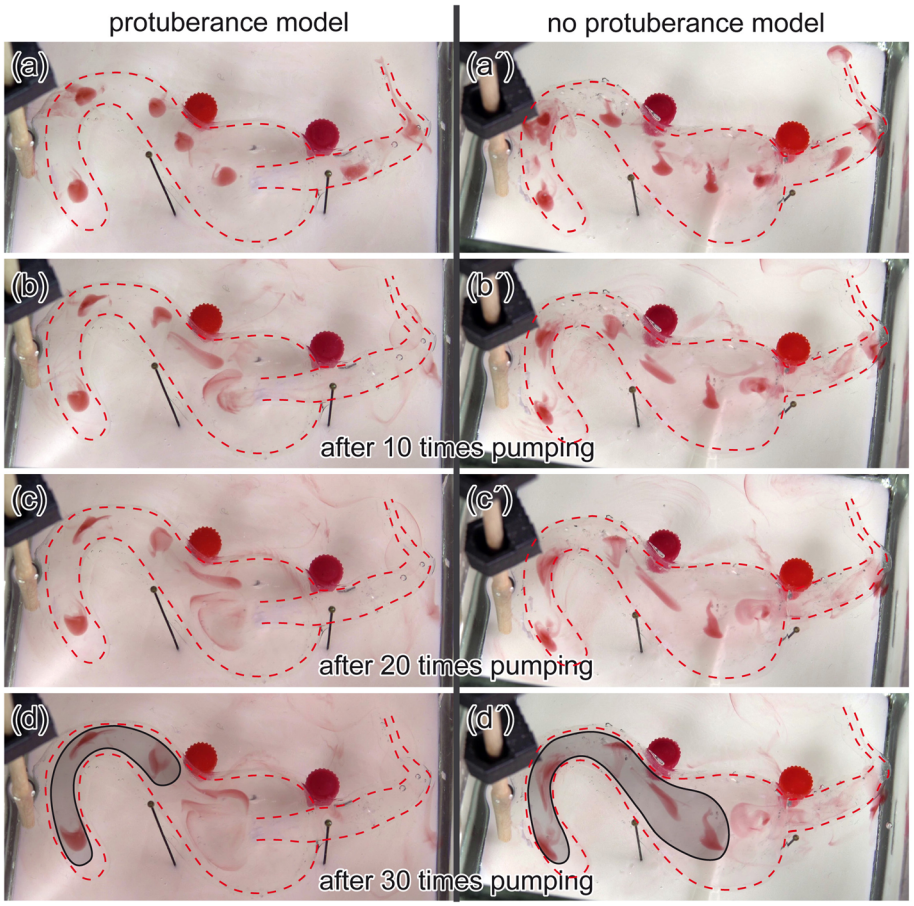

Fig. 5 Fluid dynamics in subsequent pumping cycles. **a-a'** Sudan Red in 1,2-propanediol was injected. **b-b'** After the C-arms were pumped ten times. **c-c'** After the C-arms were pumped 20 times. **d-d'** After the C-arms were pumped 30 times. The visible unmixed ink drops are marked with solid black lines

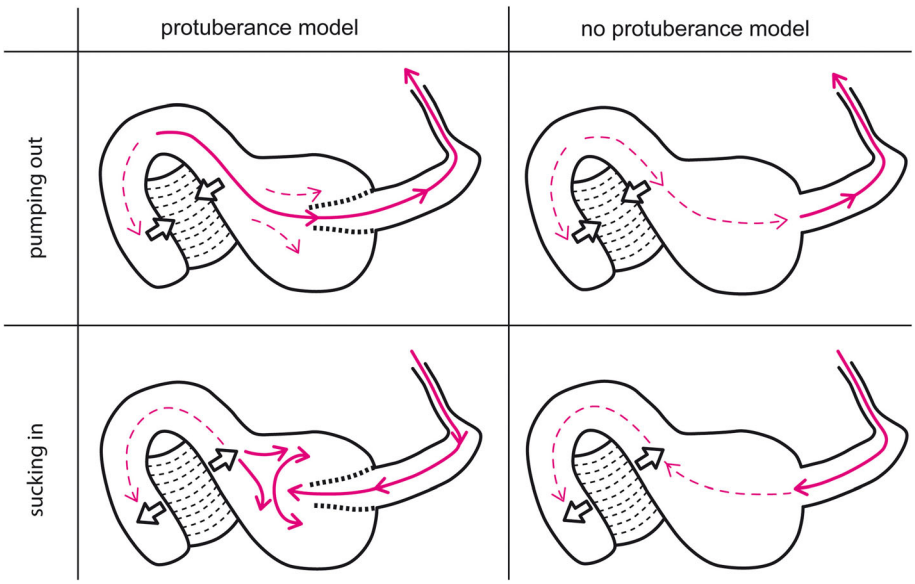

Fig. 6 Schemes of the fluid dynamics in the two models with and without the internal protuberance interpreted based on our tests. Arrows show the fluid movement. The solid lines indicate remarkable fluid movements, and the dashed lines represent possible fluid movements that are milder than the others

last male sperm precedence decreases in females with shorter remating intervals e.g., [49–51]. In *A. alni*, last male sperm precedence may be altered not only by the interval lengths but also by the timing of pumping cycles. Our experiments may suggest what could happen in the spermatheca of *A. alni* as follows. When females pump just after mating with a second male, the spermatheca with the internal protuberance explicitly pushes sperm located close to the exit/entrance out, and the sperm is only partially mixed with the previously preserved sperm in the storage chamber. This process causes low last male sperm precedence. In contrast, when females pump after ovulation, sperm adjacent to the exit/entrance may be mainly mixed with sperm in the swollen part (eggs might avoid leaking sperm out from the bursa copulatrix). Then, the last male sperm precedence increases. In practice, it is extremely challenging to test the hypothesis proposed here as a possible CFC mechanism. However, this mechanism is potentially possible.

Fluid dynamics of semen in the spermatheca are undoubtedly regulated not solely by females through the spermathecal shape because spermatozoa themselves can move [14, 42, 52]. As Lüpold and Pitnick [14] admonished in the latest review, ignorance of spermatozoa motility in vivo does not lead to correct assumptions since the motility of spermatozoa changes according to places or viscosity of a medium, in which spermatozoa swim [14, 53]. Therefore, the lack of information on the physical properties of semen results in gaps in our understanding of system functionality. Therefore, measurements of semen viscosity must be experimentally obtained to unveil the entire process of sperm dynamics. Some rheological methods previously applied for measuring viscosities of small volumes of fluids, such as those used for characterisations of insect foot secretions [54] or haemolymph of a moth [55], might be potential options for solving this problem.

It is, in fact, possible to track spermatozoa movement by using transgenic males in model species such as *Drosophila* fruit flies, the flatworm *Macrostomum lignano* and the red flour beetle *Tribolium castaneum* [56–58]. However, this technique is applicable only for model organisms frequently used in genetic experiments, and our new approach can partially compensate for this issue. Optimal genetic engineering techniques applied for model organisms should be combined with fluid dynamic tests applied for a variety of taxa. Since it has been proven that the diversity of female reproductive tracts has driven the evolution of sperm morphology [35], it could be essential to compare fluid dynamics within spermathecae of many other species. Ideally, our experimental approach using artificial 3D printed models should be combined with computational fluid dynamics simulations in the future. Such study concepts have already been successfully applied, e.g., to ascertain a passive hydrodynamic feeding mechanism in a fossil brachiopod [59–61].

Conclusion

Our fluid dynamics tests based on 3D printed spermathecae suggest that structural variations of the spermatheca strongly affect sperm dynamics, although this perspective has been largely overlooked. Moreover, our approach enables reconstructions of the evolution of CFC by focusing on the structural diversity of the spermatheca. For example, in the subfamily Criocerinae of the studied beetle family Chrysomelidae, it was estimated that the simple C-shaped type of the spermatheca found in *A. alni* and *D. crassipes* is plesiomorphic, and derived types similar to the rest of the studied species evolved independently [62]. Our approach is merely a small addition to a broad range of approaches towards understanding CFC. However, this approach is indispensable and hitherto missing in this field of reproductive biology.

Methods

Samples

The following six leaf beetle species were used in the study: *Ca. vibex* Linnaeus, 1767 (Cassidinae), *A. alni* (Linnaeus, 1758) (Galerucinae), *G. viridula* (DeGeer, 1775) (Galerucinae), *D. crassipes* Fabricius, 1775 (Donaciinae), *Cr. duodecimpunctata* (Linnaeus, 1758) (Criocerinae), and *Cr. asparagi* (Linnaeus, 1758) (Criocerinae). All beetles were collected in Kiel, Germany, between June and August 2017. In most cases, we collected adults in the field, but for *C. vibex*, larvae and pupae were also collected and maintained under laboratory conditions to obtain additional adult samples. To prepare samples, the beetles were either anaesthetised with CO_2 before dissection or frozen in a conventional freezer at − 20 °C. All beetles were dissected in 0.1 M phosphate-buffered saline (PBS; pH = 7.4; Carl Roth GmbH & Co. KG, Karlsruhe, Germany) under an Olympus SZX12 stereomicroscope (Olympus Corporation, Tokyo, Japan).

Micro-computed tomography

Specimens were fixed in 2.5% glutaraldehyde in PBS. At least two to three individuals of each species were used. They were kept in a conventional fridge (4 °C) for one night for fixation, rinsed in distilled water three times (each time for 15 min), dehydrated in an ascending series of ethanol and rinsed twice in absolute ethanol as the final step (each time for 20 min). The samples were dried using a critical point dryer (CPDA/Quorum Technologies Ltd., Kent, UK). Then, each sample was fixed on a thin-wall borosilicate glass capillary (120 × 1 mm, Hirschmann-Laborgeräte GmbH & Co. KG, Eberstadt, Germany) using a Coltène President light body kit, art.

no. 4667 (polyvinylsiloxane (PVS) elastomer) (Coltène/Whaledent Inc., USA) and scanned using a high-resolution MicroCT SkyScan 1172 system (RJL Micro & Analytic GmbH, Karlsdorf-Neuthard, Germany) with a current of 250 μA and a voltage of 40 kV for all species except for *D. crassipes*, which was scanned with a current of 175 μA and a voltage of 29 kV. Segmentation of the spermathecae was performed using the software Amira 6.2.0 (Visualization Sciences Group, Mérignac, France).

Scanning electron microscopy

The specimens were fixed in 2.5% glutaraldehyde in PBS. They were kept in a conventional refrigerator at 4 °C for one night. For this experiment, one to two individuals were used from each species. They were rinsed in distilled water three times (each time for 15 min), dehydrated in an ascending series of ethanol with absolute ethanol twice as the last step (each time for 20 min) and dried with the critical point dryer. The specimens were sputter-coated with gold-palladium (approx. 10 nm thickness) using a high vacuum sputter coater (Leica EM SCD 500; Leica Microscopy GmbH, Wetzlar, Germany) and visualised with a scanning electron microscope (Hitachi TM3000; Hitachi High-Tech Corp., Tokyo, Japan) at an accelerating voltage of 15 kV.

Confocal laser scanning microscopy

To study material gradients in the spermatheca, we applied the method developed by Michels and Gorb [43] using confocal laser scanning microscopy (CLSM). Michels and Gorb [43] visualised the autofluorescence of materials composing arthropod cuticles, and this enabled us to estimate material gradients by assigning colours to signals detected from different materials. This approach was previously justified in the feet setae of ladybird beetles by nanoindentation using atomic force microscopy (AFM) [63].

For this purpose, spermathecae were dissected out in 0.1 M PBS and rinsed in glycerin (≥99.5%, free of water, Carl Roth GmbH & Co. KG). At least two individuals were investigated for each species. Following Michels and Gorb [43], the autofluorescence of the spermathecae was visualised with a Zeiss LSM 700 confocal laser scanning microscope (Carl Zeiss Microscopy GmbH, Jena, Germany). Four stable solid-state lasers with wavelengths of 405 nm, 488 nm, 555 nm and 639 nm were used; for the detection of selective emitted autofluorescence signals, a bandpass emission filter transmitting light with wavelengths 420–480 nm and longpass emission filters transmitting light with wavelengths ≥490 nm, ≥560 nm and ≥ 640 nm were applied, respectively. An objective lens with 10× (Zeiss Plan-Apochromat, numerical aperture [NA] 0.45) magnification was used. We assigned colours to each micrograph obtained through the 420–480 nm, ≥490 nm, ≥560 nm and ≥ 640 nm filters according to the following colour code [43]: blue, green, red (50% saturation) and red (50% saturation), respectively. Based on overlaid micrographs and previous data on the stiffnesses of different types of insect cuticles [64], we interpreted the physical properties of the spermatheca as well sclerotised (red), tough and flexible (yellow to green) and resilin enriched (containing rubber-like protein) (blue). However, this is not an absolute analysis of material gradients, so red-coloured regions in two different images are not necessarily equally well sclerotized.

Preparation of models

To experimentally simulate sperm dynamics, we created enlarged, transparent and flexible spermatheca models (see Supplementary information 1 for the detailed method including method validation and practical advice). Based on a segmented digital model of *A. alni*, we prepared inner moulds using Amira software and printed them using a conventional FDM 3D printer (the Original Prusa i3 MK2S 3D printer, Prusa Research s.r.o., Prague, Czech Republic). Printing settings (layer height: 0.15 mm, perimeters: 2, infill density: 0%, supporting material: support on build plate only) were set with the software Slic3r 1.36.2-prusa3d (Prusa Research s.r.o., Prague, Czech Republic) to print the inner moulds (8 cm in height) with polylactide (PLA) polymer.

To create models using the printed inner moulds, two-component polydimethylsiloxane (PDMS), ten parts of SYLGARD® 184 silicone elastomer and one part of SYLGARD® 184 silicone elastomer curing agent (Sigma-Aldrich, St. Louis, Missouri, USA) were used. Afterwards, the mixture was kept at 65 °C for 25 min to accelerate curing and increase the viscosity. The printed model was offhand-dipped in the fluid PDMS, covered with it and hanged during a curing process at 65 °C for 40 min. This process was repeated every 40 min in total seven times to thicken the PDMS wall until it was stable enough. Later, the inner moulds covered with PLA were placed in an ultrasonic bath filled with acetone under a fume hood.

Fluid dynamics tests

To be able to use the abovementioned models for fluid dynamics tests, we upscaled the models. To simulate meaningful sperm dynamics using our models, we had to consider the Reynolds number. This number is a dimensionless quantity for predicting flow patterns, and it needed to be kept constant so that we could simulate

sperm dynamics in the upscaled models. The Reynolds number was defined by Sedov [65]:

$$\mathrm{Re} = \frac{\rho \mathrm{uL}}{\mu} = \frac{\mathrm{uL}}{\nu} \quad (1)$$

where ρ is the density of fluids ($\mathrm{kg\,m^{-3}}$), u is the velocity of fluids with respect to an object ($\mathrm{m\,s^{-1}}$), L is the characteristic linear dimension (*volume*) (m), μ is the dynamic viscosity of fluids ($\mathrm{Pa\,s^{-1}}$) and ν is the kinematic viscosity ($\nu = \frac{\mu}{\rho}$) ($\mathrm{m^2\,s^{-1}}$). Because u should be equal between the printed models and reality, the formula can be simplified to

$$\nu_{\mathrm{model}}/\nu_{\mathrm{real}} = k\frac{L_{model}}{L_{real}} \quad (2)$$

The volumes of the three-dimensionally printed models were measured using a measuring cylinder, and the volume was 16 ml ($16 \times 10^{12}\,\mu\mathrm{m}^3$). The volume of the spermatheca in *A. alni* was measured with a segmented model with a function called *material statistics* in the software Amira, and it was $14.9 \times 10^6\,\mu\mathrm{m}^3$. Therefore, the ratio of the two characteristic linear dimensions $\nu_{\mathrm{model}}/\nu_{\mathrm{real}}$ is approximately 100. The dynamic/kinematic viscosities of semen are not yet known, and semen of the studied species does not seem to be much more viscous than PBS. Therefore, for simplicity, the kinematic viscosity of the semen was assumed to be that of distilled water (ν_{water}, 20 °C = $1.002 \times 10^{-6}\,\mathrm{m^2\,s^{-1}}$ [66]), which means that our experimental medium should have a kinematic viscosity of approximately $1.0 \times 10^{-4}\,\mathrm{m^2\,s^{-1}}$. Considering accessibility, safety and convenience, we chose 1,2-propanediol (propylene glycol) ($\nu_{\mathrm{1,2\text{-}propanediol}}$, 21.1 °C = $0.52 \times 10^{-4}\,\mathrm{m^2\,s^{-1}}$ [67]) as a medium.

The above-prepared models were filled with 1,2-propanediol, and droplets of Sudan Red dissolved in 1,2-propanediol were injected into the models using disposal plastic injectors. According to the functional morphology hypothesis proposed in this study, we simulated pumping of the C-arms of the spermatheca models with gloved fingers as a first step (Supplementary information). However, with this method, it is not possible to control the velocity of each pumping cycle. We also wrote a coordinate script (Supplementary information 2, script 1) including commands to the 3D printer to move a stick contracting and relaxing the C-arms to imitate pumping cycles and carried out the experiments under the 3D printer. The fluid dynamics tests were recorded using a DSC-RX10M3 digital camera (Sony Corporation, Tokyo, Japan) with lighting provided by a Rotolight AEOS 2-Light Kit (Rotolight, Iver, UK).

Supplementary information

Supplementary information accompanies this paper at https://doi.org/10.1186/s40850-020-00058-2.

Additional file 1 Supplementary information 1.pdf. How to prepare enlarged transparent, flexible and low-cost models and validation of the method.

Additional file 2 Supplementary information 2, a script 1.txt. The script used for the fluid dynamics test described in the main text and including commands to the 3D printer to move a stick to contract and relax the C-arms of the models with an absolute velocity.

Additional file 3 Supplementary information 3, Movies.MP4. Fluid dynamics tests performed by the 3D printer.
Supplementary information 3, Movie 1. Protuberance model, first 30 pumping cycles shown. The result was recorded at 50 fps.
Supplementary information 3, Movie 2. No protuberance model, first 30 pumping cycles. The result was recorded at 50 fps.

Additional file 4 Supplementary information 4, figures.jpeg. The fluid dynamics tests (first pumping movement, outflow) were performed by the experimenter's fingers. **Supplementary information 4,** Fig. 1. Transparent flexible models and fluid dynamics tests (first pumping movement, outflow) using the *Agelastica alni* spermatheca models with a realistic internal protuberance (left column, highlighted with red dashed lines) and without the protuberance (right column). (a-a') The models fully immersed in 1,2-propanediol. (b-b') Sudan Red in 1,2-propanediol was injected. (c-e') The first pumping cycle filmed at 50 fps, and still images at different conditions are exhibited. The solid white arrows show the direction of the distal C-arm movement. The black arrows indicate a marked shift of the injected ink spots in the models. The times listed in each image are the time after pumping started. (f-f') Schemes of the observed outflow in the first pumping cycle. **Supplementary information 4,** Fig. 1 (cont.). Transparent flexible models and fluid dynamics tests (first pumping, inflow) using the *Agelastica alni* spermatheca models with a realistic internal protuberance (left column, highlighted with red dashed lines) and without the protuberance (right column). (g-h') The first pumping cycle filmed at 50 fps, with still images shown under different conditions. The solid white arrows show directions of the distal C-arm movement. The black arrows show a marked shift of the fluid in the models. (i-i') The inflow at the second pumping cycle. (j-j') Schemes of the observed inflow during the first two pumping cycles. The light-pink circles in the schemes indicate the original locations of the injected ink. **Supplementary information 4,** Fig. 2. Fluid dynamics in subsequent pumping cycles. (a-a') Sudan Red in 1,2-propanediol was injected. (b-b') After the C-arms were pumped ten times. (c-c') After the C-arms were pumped 20 times, but in the protuberance model at the 11th pumping cycle, Sudan Red partly leaked (Supplementary Information 5, Movie 2) from a lateral crack. However, similar results were observed before the lateral crack occurred. (d-d') After the C-arms were pumped 30 times. The visible unmixed ink drops are marked with solid black lines.

Additional file 5 Supplementary information 5, Movies.MP4. Fluid dynamics tests performed by experimenter's fingers.
Supplementary information 5, Movie 1. Protuberance model, first ten pumping cycles. The result was recorded at 50 fps.
Supplementary information 5, Movie 2. Protuberance model, during 20–30 pumping cycles. The result was recorded at 50 fps.
Supplementary information 5, Movie 3. No protuberance model, first ten pumping cycles. The result was recorded at 50 fps.
Supplementary information 5, Movie 4. No protuberance model, during 20–30 pumping cycles. The result was recorded at 50 fps.

Abbreviations

AFM: Atomic force microscopy; CFC: Cryptic female choice; CLSM: Confocal laser scanning microscopy; μCT: Micro-computed tomography; PCMC: Postcopulatory mate choice; PCSS: Postcopulatory sexual selection; PDMS: Polydimethylsiloxane; PLA: Polylactide

Acknowledgements

We are grateful to H. Rajabi (Kiel University, Germany) for discussions about viscosity calculations and to J. Michels (Kiel University, Germany) for technical

help and advice regarding muscle visualisations. We also thank T. Büscher (Kiel University, Germany) for help with species identifications, D.S. Petersen (Kiel University, Germany) for technical support with handling PDMS and S. Büsse (Kiel University, Germany) for technical advice regarding analysing our samples using μCT. N. Bijma and F. Bäumler (Kiel University, Germany) gave us information regarding the video recordings. E. Appel and S. Ito (Kiel University, Germany) provided invaluable comments on the staining method.

Authors' contributions

YM and SNG conceptualised the study, YM, SG and HTT performed the experiments, YM and SG wrote the draft, and HTT and SNG revised it. The authors contributed to and approved the final draft of the manuscript.

Funding

This study was supported by the German Research Foundation (DFG grant numbers MA 7400/1–1) to YM. The funder had no role in the study design, data collection and analysis, decision to publish, or preparation of the manuscript.

Availability of data and materials

All supporting data are available as supplementary materials except for micro-CT data, which are available from the corresponding author upon reasonable request.

Ethics approval and consent to participate

No permissions for research ethics or from animal ethics committees were necessary since in our study, only unregulated insect species were examined.

Consent for publication

Not applicable.

Competing interests

We declare no competing interests.

Received: 17 December 2019 Accepted: 2 July 2020
Published online: 28 July 2020

References

1. Taylor ML, Price TAR, Wedell N. Polyandry in nature: a global analysis. Trends Ecol Evol. 2014;29:376–83.
2. Orr TJ, Brennan PL. Sperm storage: distinguishing selective processes and evaluating criteria. Trends Ecol Evol. 2015;30:261–72.
3. Orr TJ, Zuk M. Sperm storage. Curr Biol. 2012;22:R8–10.
4. Dougherty LR, Simmons LW, Shuker DM. Postcopulatory sexual selection when a female mates once. Anim Behav. 2016;116:13–6.
5. Eberhard WG. Female control: sexual selection by cryptic female choice. Princeton: Princeton University Press; 1996.
6. Firman RC, Gasparini C, Manier MK, Pizzari T. Postmating female control: 20 years of cryptic female choice. Trends Ecol Evol. 2017;32:368–82.
7. Parker GA. Sperm competition and its evolutionary consequences in the insects. Biol Rev. 1970;45:525–67.
8. Simmons LW. Sperm competition and its evolutionary consequences in the insects. Princeton: Princeton University Press; 2001.
9. Arnqvist G, Rowe L. Sexual conflict. Princeton: Princeton University Press; 2005.
10. Eberhard WG, Lehmann GUC. Demonstrating sexual selection by cryptic female choice on male genitalia: what is enough? Evolution. 2019;73:2415–35.
11. Thornhill R. Cryptic female choice and its implications in the scorpionfly *Harpobittacus nigriceps*. Am Nat. 1983;122:765–88.
12. Arnqvist G. Cryptic female choice. In: Shuker D, Simmons L, editors. The evolution of insect mating systems. Oxford: Oxford University Press; 2014. p. 204–20.
13. Eberhard WG. Cryptic female choice and other types of post-copulatory sexual selection. In: Peretti AV, Aisenberg A, editors. Cryptic female choice in arthropods. Cham and New York: Springer; 2015. p. 1–26.
14. Lüpold S, Pitnick S. Sperm form and function: what do we know about the role of sexual selection? Reproduction. 2018;155:R229–43.
15. Simmons LW. Sexual selection and genital evolution. Aust Entomol. 2014;53:1–17.
16. Brennan PLR, Prum RO. The limits of sexual conflict in the narrow sense: new insights from waterfowl biology. Philos Trans R Soc. 2012;367:2324–38.
17. Pizzari T, Birkhead TR. Female feral fowl eject sperm of subdominant males. Nature. 2000;405:787–9.
18. Helfenstein F, Wagner RH, Danchin E. Sexual conflict over sperm ejection in monogamous pairs of kittiwakes *Rissa tridactyla*. Behav Ecol Sociobiol. 2003; 54:370–6.
19. Rodriguez V. Copulatory courtship in *Chelymorpha alternans* Boheman (Coleoptera: Chrysomelidae: Cassidinae). Coleopt Bull. 1995;49:327–31.
20. Peretti AV, Eberhard WG. Cryptic female choice via sperm dumping favours male copulatory courtship in a spider. J Evol Biol. 2010;23:271–81.
21. Eberhard WG. Postcopulatory sexual selection: Darwin's omission and its consequences. Proc Natl Acad Sci U S A. 2009;106:10025–32.
22. Ah-King M, Barron AB, Herberstein ME. Genital evolution: why are females still understudied? PLoS Biol. 2014;12:e1001851.
23. Sloan NS, Simmons LW. The evolution of female genitalia. J Evol Biol. 2019; 32:882–99.
24. Pascini TV, Martins GF. The insect spermatheca: an overview. Zoology. 2017; 121:56–71.
25. Manier MK, Lüpold S, Pitnick S, Starmer WT. An analytical framework for estimating fertilization bias and the fertilization set from multiple sperm-storage organs. Am Nat. 2013;182:552–61.
26. Ward PI. Cryptic female choice in the yellow dung fly *Scathophaga stercoraria* (L.). Evolution. 2000;54:1680–6.
27. Bloch Qazi MG, Aprille JR, Lewis SM. Female role in sperm storage in the red flour beetle, *Tribolium castaneum*. Comp Biochem Physiol A Mol Integr Physiol. 1998;120:641–7.
28. Rodriguez V. Function of the spermathecal muscle in *Chelymorpha alternans* Boheman (Coleoptera: Chrysomelidae: Cassidinae). Physiol Entomol. 1994;19: 198–202.
29. Villavaso EJ. Functions of the spermathecal muscle of the boll weevil, *Anthonomus grandis*. J Insect Physiol. 1975;21:1275–8.
30. Bordy B, Doguet S. Contribution à la connaissance des Cassidinae de France. Étude de leur spermathèque (Coleoptera, Chrysomelidae). Nouv Rev Entomol. 1987;2:161–76.
31. Lackner T, Tarasov S. Female genitalia are moderately informative for phylogenetic inference and not concerted with male genitalia in Saprininae beetles (Coleoptera. Histeridae). Syst Entomol. 2019;44:667–85.
32. Pluot-Sigwalt D, Lis JA. Morphology of the spermatheca in the Cydnidae (Hemiptera: Heteroptera): bearing of its diversity on classification and phylogeny. Eur J Entomol. 2008;105:279–312.
33. Rodríguez-Mirón GM, Zaragoza-Caballero S, López-Pérez S. Comparative morphology of the spermatheca in Megalopodidae (Coleoptera, Chrysomeloidea). ZooKeys. 2017;720:47–64.
34. Surtees G. Spermathecal structure in some Coleoptera associated with stored products. Proc R Entomol Soc A. 1961;36:144–52.
35. Higginson DM, Miller KB, Segraves KA, Pitnick S. Female reproductive tract form drives the evolution of complex sperm morphology. Proc Natl Acad Sci U S A. 2012;109:4538–43.
36. Brennan PLR, Prum RO. Mechanisms and evidence of genital coevolution: the roles of natural selection, mate choice, and sexual conflict. CSH Perspect Biol. 2015;7:a017749.
37. Fedina TY, Lewis SM. An integrative view of sexual selection in *Tribolium* flour beetles. Biol Rev. 2008;83:151–71.
38. Brennan PLR. Studying genital coevolution to understand intromittent organ morphology. Integr Comp Biol. 2016;56:669–81.
39. Kelly DA. Intromittent organ morphology and biomechanics: defining the physical challenges of copulation. Integr Comp Biol. 2016;56:630–4.
40. Chaboo CS. Biology and phylogeny of the Cassidinae Gyllenhal Sensu Lato (tortoise and leaf-mining beetles) (Coleoptera: Chrysomelidae). Bull Am Mus Nat Hist. 2007;305:1–250.
41. Matsumura Y, Suzuki K. Comparative morphology of internal reproductive systems in leaf beetles of the Donaciinae and Criocerinae (Coleoptera: Chrysomelidae) and its implication for the phylogeny. Zootaxa. 1845;2008:1–32.
42. Werner M, Simmons LW. Insect sperm motility. Biol Rev. 2008;83:191–208.
43. Michels J, Gorb SN. Detailed three-dimensional visualization of resilin in the exoskeleton of arthropods using confocal laser scanning microscopy. J Microsc. 2012;245:1–16.
44. Schärer L, Littlewood DTJ, Waeschenbach A, Yoshida W, Vizoso DB. Mating behavior and the evolution of sperm design. Proc Natl Acad Sci U S A. 2011;108:1490–5.
45. Tanabe T, Sota T. Both male and female novel traits promote the correlated evolution of genitalia between the sexes in an arthropod. Evolution. 2013; 68:441–52.

46. Michels J, Appel E, Gorb SN. Functional diversity of resilin in Arthropoda. Beilstein J Nanotechnol. 2016;7:1241–59.
47. Gomez-Zurita J, Hunt T, Vogler AP. Multilocus ribosomal RNA phylogeny of the leaf beetles (Chrysomelidae). Cladistics. 2008;24:34–50.
48. Zucht G. Zur Biologie von *Agelastica alni* L. Deut Entomol Z. 1934;3–4:145–218.
49. Bernasconi G, Brostaux Y, Meyer EP, Arnaud L. Do spermathecal morphology and inter-mating interval influence paternity in the polyandrous beetle *Tribolium castaneum*? Behaviour. 2006;143:643–58.
50. Hook KA. Female remating decisions and a shorter inter-mating interval diminish last-male sperm precedence. Behav Ecol Sociobiol. 2017;71:2089.
51. Laturney M, van Eijk R, Billeter J-C. Last male sperm precedence is modulated by female remating rate in *Drosophila melanogaster*. Evol Lett. 2018;2:180–9.
52. Gaffney EA, Gadêlha H, Smith DJ, Blake JR, Kirkman-Brown JC. Mammalian sperm motility: observation and theory. Annu Rev Fluid Mech. 2011;43:501–28.
53. Teran J, Fauci L, Shelley M. Viscoelastic fluid response can increase the speed and efficiency of a free swimmer. Phys Rev Lett. 2010;104:38101.
54. Peisker H, Heepe L, Kovalev AE, Gorb SN. Comparative study of the fluid viscosity in tarsal hairy attachment systems of flies and beetles. J R Soc Interface. 2014;11:20140752.
55. Kenny MC, Giarra MN, Granata E, Socha JJ. How temperature influences the viscosity of hornworm hemolymph. J Exp Biol. 2018;221:jeb.186338.
56. Droge-Young EM, Belote JM, Perez GS, Pitnick S. Resolving mechanisms of short-term competitive fertilization success in the red flour beetle. J Insect Physiol. 2016;93:1–10.
57. Manier MK, Belote JM, Berben KS, Novikov D, Stuart WT, Pitnick S. Resolving mechanisms of competitive fertilization success in *Drosophila melanogaster*. Science. 2010;328:354–7.
58. Marie-Orleach L, Janicke T, Vizoso DB, Eichmann M, Schärer L. Fluorescent sperm in a transparent worm: validation of a GFP marker to study sexual selection. BMC Evol Biol. 2014;14:148.
59. Shiino Y, Kuwazuru O. Functional adaptation of spiriferide brachiopod morphology. J Evol Biol. 2010;23:1547–57.
60. Shiino Y, Kuwazuru O. Theoretical approach to the functional optimisation of spiriferide brachiopod shell: optimum morphology of sulcus. J Theor Biol. 2011;276:192–8.
61. Shiino Y, Suzuki Y. The ideal hydrodynamic form of the concavo-convex productide brachiopod shell. Lethaia. 2011;44:329–43.
62. Matsumura Y, Yao I, Beutel RG, Yoshizawa K. Molecular phylogeny of the leaf beetle subfamily Criocerinae (Coleoptera: Chrysomelidae) and the correlated evolution of reproductive organs. Arthropod Syst Phylo. 2014;72:95–110.
63. Peisker H, Michels J, Gorb SN. Evidence for a material gradient in the adhesive tarsal setae of the ladybird beetle *Coccinella septempunctata*. Nat Commun. 2013;4:1661.
64. Eshghi SH, Jafarpour M, Darvizeh A, Gorb SN, Rajabi H. A simple, high-resolution, non-destructive method for determining the spatial gradient of the elastic modulus of insect cuticle. J R Soc Interface. 2018;15:20180312.
65. Sedov LI. Similarity and dimensional methods in mechanics. 1st ed. Cambridge: Academic Press; 1959.
66. Engineering ToolBox: Water - dynamic and kinematic viscosity. 2004 https://www.engineeringtoolbox.com/water-dynamic-kinematic-viscosity-d_596.html. Accessed 10 Dec 2018.
67. Engineering ToolBox: Liquids - kinematic viscosities. 2003 https://www.engineeringtoolbox.com/kinematic-viscosity-d_397.html. Accessed 10 Dec 2018.

Publisher's Note